Chinese Chemical Letters 32 (2021) 594–597

Contents lists available at ScienceDirect

Chinese Chemical Letters

journal homepage: www.elsevier.com/locate/cclet

Communication

Free-standing nitrogen doped graphene/$Co(OH)_2$ composite films with superior catalytic activity for aprotic lithium-oxygen batteries

Zifang Zhao[a,b], Yue Liu[b], Fang Wan[b], Shuai Wang[b], Nannan Zhang[b], Lili Liu[a,*], Anyuan Cao[c], Zhiqiang Niu[b,*]

[a] Tianjin Key Laboratory for Photoelectric Materials and Devices, School of Materials Science and Engineering, Tianjin University of Technology, Tianjin 300384, China
[b] Key Laboratory of Advanced Energy Materials Chemistry (Ministry of Education), Renewable Energy Conversion and Storage Center, College of Chemistry, Nankai University, Tianjin 300071, China
[c] Department of Materials Science and Engineering, College of Engineering, Peking University, Beijing 100871, China

ARTICLE INFO

Article history:
Received 12 October 2020
Received in revised form 6 November 2020
Accepted 17 November 2020
Available online 30 November 2020

Keywords:
Free-standing films
Nitrogen doping
Graphene
$Co(OH)_2$
Lithium-oxygen batteries

ABSTRACT

The recent boom in large-scale energy storage system promotes the development of lithium-oxygen batteries because of their high theoretical energy density. However, their applications are still limited by the sluggish kinetic, insoluble discharge product deposition and the undesired parasitic reaction. Herein, the free-standing nitrogen doped reduced graphene oxide/$Co(OH)_2$ (NRGO/$Co(OH)_2$) composite films were prepared by a facile hydrothermal method. The NRGO/$Co(OH)_2$ composite films display interconnected three-dimensional conductive network, which can not only promote the diffusion of O_2 and the transport of electrolyte ions, but also provide abundant storage space for discharge products. Moreover, the introduction of nitrogen-containing functional groups results in improved conductivity and electron adsorption ability, which can facilitate electron transport and enhance the surface catalytic activity. Combining with excellent catalytic performance, the lithium-oxygen batteries with NRGO/$Co(OH)_2$ composite film cathodes deliver low charge overpotential and excellent cycling performance.

Rechargeable energy storage devices with high energy density have attracted much attention due to the increasing demand for energy and the gradual expenditure of conventional fossil energy sources [1–3]. Lithium-oxygen batteries (LOBs) are promising energy storage devices because of their much higher energy density than the conventional lithium-ion batteries [4–7]. However, LOBs often suffer from low round-trip efficiency, poor cycle life and voltage decay [8–11]. It has been revealed that this limited electrochemical performance often arises from the unwanted parasitic side reactions involving the air cathode and electrolyte [12–15]. In particular, the attack of oxygen radicals to cathode and electrolyte is their major origin [16,17]. During the discharge process, Li^+ ions gradually react with oxygen to form solid Li_2O_2 products in the cathode. The insoluble Li_2O_2 will decrease the active area of the cathode, and thus block the diffusion pathway of oxygen and Li^+ [18,19]. Hence, in order to enhance the electrochemical performance of LOBs, it is essential to prepare electrocatalysts with high activity as well as design the cathode configurations with coordinated triphase (electrolyte, oxygen and electrocatalyst) reactive sites.

To date, a variety of electrocatalysts have been explored to improve the electrochemical performance of LOBs. Rare metals, such as Pt, Ir, Ru and Pd, exhibit excellent catalytic activity for oxygen reduction/evolution reactions (ORRs/OERs) in LOBs [20–24]. Nevertheless, the high cost of the materials hinders their applications. As a result, it is highly desired to discover efficient and low-cost electrocatalysts for LOBs [25,26]. Transition metal cobalt-based catalysts are widely used in LOBs due to their low cost, environmentally friendliness and favorable co-catalyst activity for both ORRs and OERs processes [27–33]. Among them, layered cobalt hydroxide is widely used as catalyst material in fields such as sensors, water splitting and OERs due to its high electrochemical redox activity and large interlayer spacing [34–36]. Therefore, it shows great potential as the electrocatalyst for aprotic LOBs.

Apart from electrocatalysts, the establishment of well-balanced triphase reaction interface also has great effects on the electrochemical performance of LOBs. The conventional LOBs cathodes are often prepared by mixing the electrocatalysts with conductive additives and polymer binders followed by casting them onto

* Corresponding authors.
E-mail addresses: lililiuhappy@163.com (L. Liu), zqniu@nankai.edu.cn (Z. Niu).

https://doi.org/10.1016/j.cclet.2020.11.047
1001-8417/

porous current collectors. As a result of the addition of polymer binders and the unsatisfactory porous structure, the diffusion of O_2 and the transport of electrolyte in traditional cathodes are limited [37–39]. Moreover, polymer binders may react with aggressive species created during discharge and charge processes, resulting in irreversible side reactions. Thus, porous and binder-free cathodes with excellent electrocatalytic activity could be considered for improving the sluggish reaction kinetics of LOBs.

In this work, we developed a facile hydrothermal strategy to fabricate free-standing nitrogen doped reduced graphene oxide/Co$(OH)_2$ (NRGO/Co$(OH)_2$) composite film cathodes. Such cathodes have the following merits: (i) high conductivity of nitrogen doped reduced graphene oxide (NRGO) facilitates electron transport; (ii) The improved electron adsorption ability generated from the nitrogen-containing functional groups results in enhanced surface catalytic activity; (iii) the large specific surface area of NRGO provides adequate catalytic sites for both ORRs and OERs processes and abundant space for accommodating discharge products; (iv) Three-dimensional (3D) interconnected NRGO network provides well-balanced triphase interface for the transport of electrolyte ions and the diffusion of O_2. Therefore, the LOBs based on NRGO/Co$(OH)_2$ composite film cathodes exhibit superior cycle performance with a highly decreased overpotential.

Fig. 1a schematically shows the fabrication process of NRGO/Co$(OH)_2$ composite foam. In a typical experiment, the Co$(OH)_2$ sheets were first uniformly mixed with the well-dispersed GO suspension by ultrasonication treatment. After further hydrothermal procedure, the free-standing NRGO/Co$(OH)_2$ composite foam with approximately 20 wt% Co$(OH)_2$ was obtained (Fig. S1 in Supporting information). However, the NRGO/Co$(OH)_2$ composite foam is too thick to be directly used as the electrode of LOBs. Therefore, it was cut and mechanically pressed into free-standing and binder-free films (Fig. 1b). The X-ray diffraction (XRD) patterns of the as-prepared Co$(OH)_2$ sheets and composite films are presented in Fig. 1c. The diffraction peaks of Co$(OH)_2$ sheets perfectly match with the hexagonal β-Co$(OH)_2$ (a = 0.3183 nm, c = 0.4652 nm, JCPDS No. 30-0443), confirming the successful synthesis of Co$(OH)_2$. However, it is noted that no peaks assigning to Co$(OH)_2$ are detected in the XRD spectrum of NRGO/Co$(OH)_2$ composite films with the mass ratio of NRGO:Co$(OH)_2$ > 3:1, indicating the well packing of Co$(OH)_2$ in NRGO. However, with the increase of Co$(OH)_2$ content in the NRGO/Co$(OH)_2$ composite films, the peaks belonging to Co$(OH)_2$ sheets appear gradually, revealing that the hydrothermal process nearly has no influence on the crystalline phase of β-Co$(OH)_2$ (Fig. S2 in Supporting information). Fig. 1d reveals the transmission electron microscopy (TEM) image and the elemental mappings of Co$(OH)_2$ sheet, which exhibit the uniform distribution of Co and O elements. The morphology of the Co$(OH)_2$ nanosheets can also be suggested by their scanning electron microscopy (SEM) images, as displayed in Figs. 2a and b.

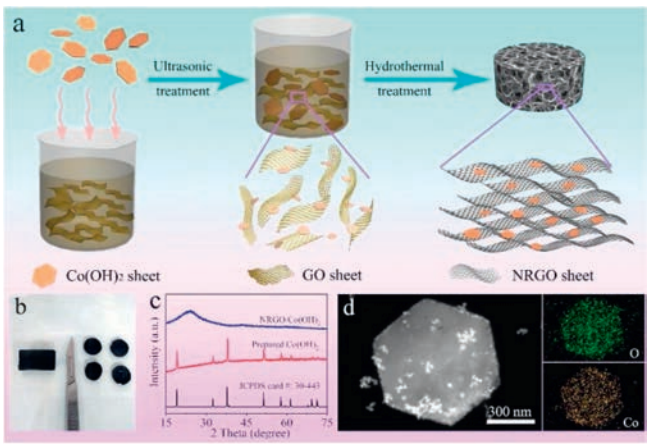

Fig. 1. (a) Schematic illustration of fabricating free-standing NRGO/Co$(OH)_2$ composite foam. (b) Optical image of NRGO/Co$(OH)_2$ samples. (c) XRD patterns of the Co$(OH)_2$ sheets and NRGO/Co$(OH)_2$ composite films. (d) TEM elemental mappings of Co$(OH)_2$ sheets.

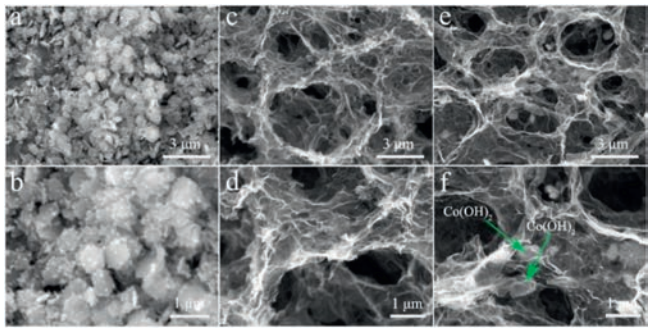

Fig. 2. SEM images of (a, b) Co$(OH)_2$ sheets, (c, d) NRGO foam and (e, f) NRGO/Co$(OH)_2$ composite foam.

As shown in Figs. 2c and d, the pure NRGO films possess a 3D porous network with pore size ranging from sub-micrometer to several micrometers. The cross-linked porous architecture can not only transport electrons, but also provide efficient pathways to ensure the diffusion of electrolyte. Moreover, such a porous structure can avoid the restacking of NRGO. Therefore, it will be favorable carrier of electrocatalysts for LOBs. After Co$(OH)_2$ was incorporated into this porous structure, NRGO/Co$(OH)_2$ composite could be obtained. The Co$(OH)_2$ nanosheets are well distributed in the porous skeleton of NRGO (Figs. 2e and f). In addition, the SEM elemental mapping images of NRGO/Co$(OH)_2$ composite verify the presence and homogeneous distribution of Co, O and C on NRGO sheets (Fig. S3 in Supporting information). Such cross-linked porous architecture not only benefits to the electrolyte ions transport and O_2 diffusion, but also provides adequate space for Li_2O_2 deposition.

The X-ray photoelectron spectroscopy (XPS) was performed to further understand the surface compositions and chemical states of the NRGO films, Co$(OH)_2$, and NRGO/Co$(OH)_2$ composite films. The survey spectrum of NRGO/Co$(OH)_2$ demonstrates the existence of Co, C, N and O elements in the composite (Fig. S4 in Supporting information), agreeing well with the XRD and EDS results above.

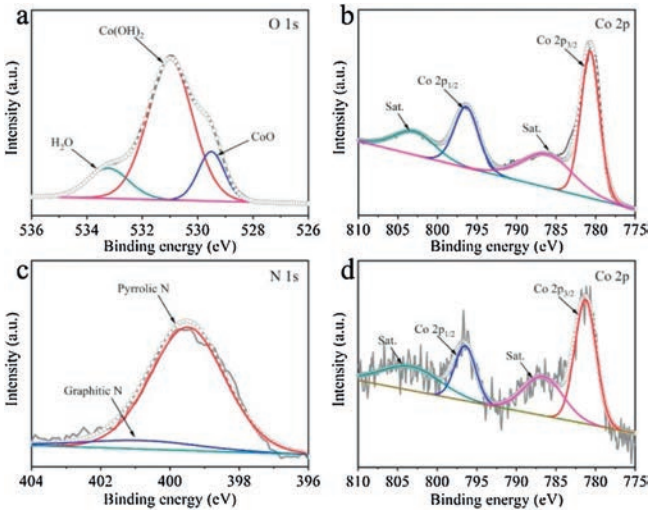

Fig. 3. (a) O 1s and (b) Co 2p XPS spectra of Co$(OH)_2$ sheets. (c) N 1s and (d) Co 2p XPS spectra of NRGO/Co$(OH)_2$ composite films.

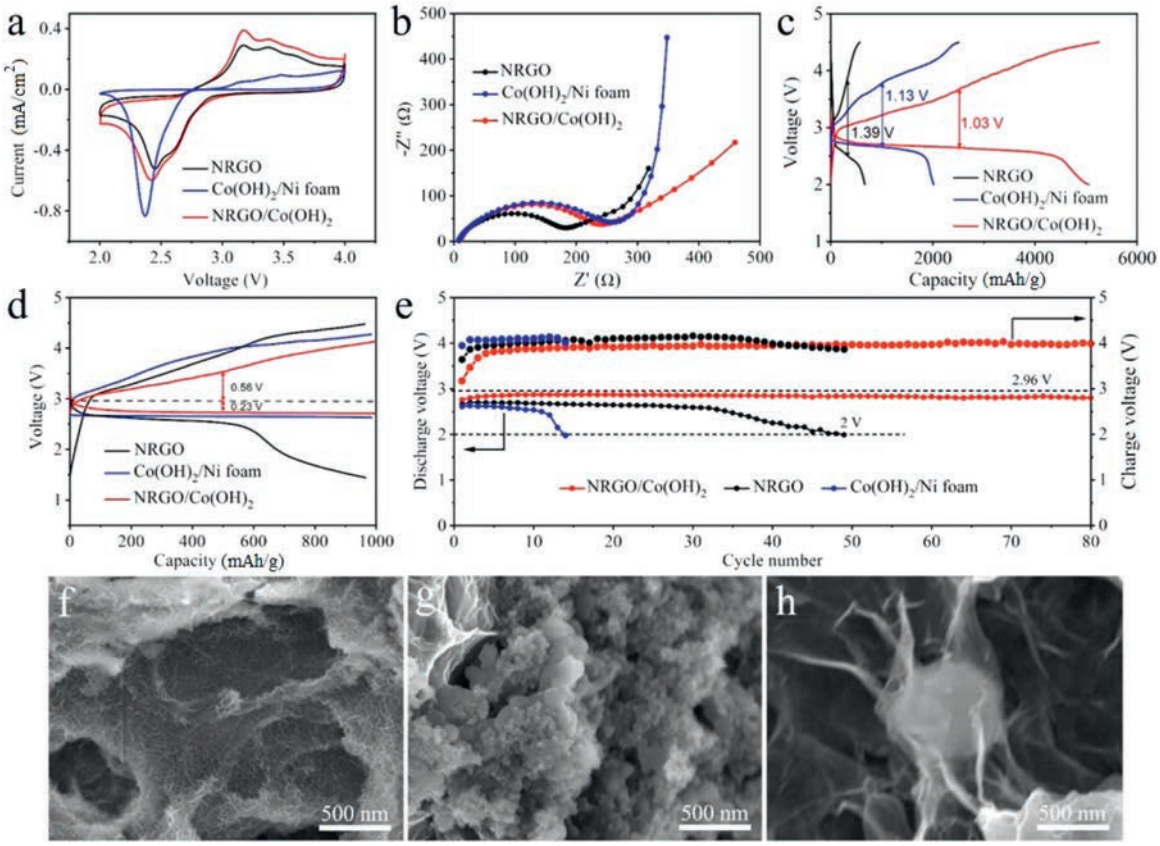

Fig. 4. (a) CV curves of NRGO films, $Co(OH)_2$/Ni foam, and NRGO/$Co(OH)_2$ composite film electrodes at a scan rate of 0.1 mV/s. (b) Nyquist plots of NRGO films, $Co(OH)_2$/Ni foam and NRGO/$Co(OH)_2$ composite film electrodes from 100 mHz to 100 kHz. (c) Full discharge/charge profiles for the first cycle of NRGO films, $Co(OH)_2$/Ni foam and NRGO/$Co(OH)_2$ composite film electrodes at the current density of 0.1 A/g. (d) Comparison of the initial discharge/charge profiles and (e) cycling performance of the LOBs with a cutoff capacity of 1000 mAh/g for NRGO films, $Co(OH)_2$/Ni foam and NRGO/$Co(OH)_2$ composite film electrodes at the current density of 0.1 A/g. SEM images of NRGO/$Co(OH)_2$ composite film electrodes at different charge/discharge states: (f) discharged to 1500 mAh/g, (g) fully discharged, and (h) recharged.

The O 1s, Co 2p and N 1s spectra are exhibited in Figs. 3a–d. The peak located at 531.1 eV reveals the existence of $Co(OH)_2$ and the shoulder peak centered at 533.2 eV can be assigned to structural water. In addition, as a result of the dehydroxylation upon drying, a shoulder peak (529.5 eV) corresponding to CoO can be also detected. Furthermore, the two main peaks centered at 780.5 eV for Co $2p_{3/2}$ and 796.0 eV for Co $2p_{1/2}$ can be ascribed to Co^{2+} [40]. Their splitting value is 15.5 eV, demonstrating the existence of Co^{2+} in $Co(OH)_2$ and NRGO/$Co(OH)_2$ composite films [41]. In addition, two different peaks centered at 399.5 and 400.9 eV in the N 1s XPS spectrum are ascribed to pyrrolic N and graphitic N, respectively. These nitrogen-containing functional groups will introduce extra electrons and promote the formation of disordered carbon nanostructures, thus significantly enhancing the O_2 adsorption on the surface of graphene [42,43].

The electrochemical performance of NRGO/$Co(OH)_2$ composite films as the electrocatalyst of LOBs was tested in coin cells. Cyclic voltammetry (CV) cures were first performed to investigate the electrocatalytic activity of NRGO/$Co(OH)_2$ composite films at a scan rate of 0.1 mV/s (Fig. 4a). Compared with NRGO films and $Co(OH)_2$/Ni foam, NRGO/$Co(OH)_2$ composite films demonstrate a higher OER peak current density, suggesting that the 3D NRGO/$Co(OH)_2$ composite films possess higher OER electrocatalytic activity to enhance the conversion between Li_2O_2 and O_2. As a result of highly conductive 3D interconnected network structure, the impedance of NRGO/$Co(OH)_2$ composite films demonstrate only a slight increase compared with that of NRGO films (Fig. 4b). In addition, NRGO/$Co(OH)_2$ composite electrodes were also studied by full discharge/charge test. Fig. 4c shows the first full discharge/charge profiles of LOBs with NRGO, $Co(OH)_2$/Ni foam and NRGO/$Co(OH)_2$ composite film electrodes at the current density of 0.1 A/g. Specifically, the discharge capacity of NRGO/$Co(OH)_2$ composite films is 5046 mAh/g, which is much higher than that of NRGO films (667 mAh/g) and $Co(OH)_2$/Ni foam (2026 mAh/g). It is shown that the NRGO/$Co(OH)_2$ composite film electrode exhibits significantly reduced overpotential (1.03 V), which is obviously lower than that of NRGO film (1.39 V), $Co(OH)_2$/Ni foam (1.13 V) as well as many other Co-based electrocatalysts [27–31]. Furthermore, the NRGO/$Co(OH)_2$ composite film electrodes exhibit obvious lower charge voltage plateau and higher discharge voltage plateau in comparison with these of NRGO film and $Co(OH)_2$/Ni foam electrodes (Fig. 4d and Fig. S5 in Supporting information). The low overpotential of NRGO/$Co(OH)_2$ composite films is able to enhance the energy efficiency of LOBs, further suggesting that NRGO/$Co(OH)_2$ composite films could offer abundant catalytic active sites to promote the Li_2O_2 formation and decomposition. Apart from their low overpotential and high capacity, the LOBs with the NRGO/$Co(OH)_2$ composite film electrodes also exhibit excellent cycle stability. As shown in Fig. 4e, LOBs with the NRGO/$Co(OH)_2$ composite film electrodes retain a stable terminal discharge above 2.0 V after 80 cycles.

The morphology change of the cathodes during different discharge-charge states were further investigated with *ex-situ* SEM. It is noted that the surface of cathode discharged to 1500 mAh/g was uniformly covered with muddy layer of Li_2O_2 (Fig. 4f). Moreover, at fully discharged state, the Li_2O_2 particles piled up and covered the entire surface of cathode (Fig. 4g). However, the discharge products were decomposed and nearly

recovered the morphology of the original state after recharging process, revealing the good rechargeability of this cathode (Fig. 4h).

In summary, free-standing NRGO/Co$(OH)_2$ composite films were prepared by a facile hydrothermal method and applied as the cathode electrocatalysts for LOBs. The free-standing NRGO/Co$(OH)_2$ composite films display unique 3D interconnected architecture, high conductivity, and superior catalytic activity, which can not only facilitate fast transport of electrons and ions as well as the diffusion of O_2, but also provide abundant storage space for discharge products. Furthermore, the introduction of nitrogen-containing functional groups induces improved electron adsorption ability, which provides more catalytic active sites for both ORR and OER processes. As a result, the NRGO/Co$(OH)_2$ composite film electrodes deliver a lower overpotential, higher discharge capacity, and an enhanced cycle life compared with NRGO and Co$(OH)_2$/Ni foam based electrodes. Therefore, such unique design could pave the way towards designing and developing efficient cathode catalysts with favorable rechargeability and cyclability for LOBs.

Declaration of competing interest

The authors declare that they have no known competing financial interests or personal relationships that could have appeared to influence the work reported in this paper.

Acknowledgments

This work was supported by Ministry of Science and Technology of China (No. 2017YFA0206701), National Natural Science Foundation of China (Nos. 51822205 and 21875121) and China Postdoctoral Science Foundation (No. 2019M650045).

Appendix A. Supplementary data

Supplementary material related to this article can be found, in the online version, at doi:https://doi.org/10.1016/j.cclet.2020.11.047.

References

[1] Z. Zhao, X. Wang, M. Yao, et al., Chin. Chem. Lett. 30 (2019) 915–918.
[2] R. Wang, M. Yao, Z. Niu, InfoMat 2 (2019) 113–125.
[3] F. Wan, J. Zhu, S. Huang, Z. Niu, Batter. Supercaps 3 (2020) 323–330.
[4] J. Gao, X. Cai, J. Wang, et al., Chem. Eng. J. 352 (2018) 972–995.
[5] Z. Chang, J. Xu, X. Zhang, Adv. Energy Mater. 7 (2017) 1700875.
[6] K.N. Jung, J. Kim, Y. Yamauchi, et al., J. Mater. Chem. A 4 (2016) 14050–14068.
[7] J.B. Park, S.H. Lee, H.G. Jung, D. Aurbach, Y.K. Sun, Adv. Mater. 30 (2018) 1704162.
[8] A.C. Luntz, B.D. McCloskey, Chem. Rev. 114 (2014) 11721–11750.
[9] F. Cheng, J. Chen, Chem. Soc. Rev. 41 (2012) 2172–2192.
[10] J. Wang, J. Liu, Y. Cai, et al., ChemElectroChem 5 (2018) 1702–1707.
[11] W. Chen, Y.F. Gong, J.H. Liu, Chin. Chem. Lett. 28 (2017) 709–718.
[12] Z. Peng, S.A. Freunberger, Y. Chen, P.G. Bruce, Science 337 (2012) 563–566.
[13] Y. Peng, Y. Zhang, J. Huang, et al., Carbon 124 (2017) 23–33.
[14] Y. Dong, S. Li, S. Hong, L. Wang, B. Wang, Chin. Chem. Lett. 31 (2020) 635–642.
[15] J. Xu, Z. Wang, D. Xu, L. Zhang, X. Zhang, Nat. Commum. 4 (2013) 2438.
[16] F. Li, T. Zhang, H. Zhou, Energy Environ. Sci. 6 (2013) 1125–1141.
[17] D. Aurbach, B.D. McCloskey, L.F. Nazar, P.G. Bruce, Nat. Energy 1 (2016) 16128.
[18] P. Tan, M. Liu, Z. Shao, M. Ni, Adv. Energy Mater. 7 (2017) 1602674.
[19] Z. Huang, H. Zeng, M. Xie, et al., Angew. Chem. Int. Ed. 58 (2019) 2345–2349.
[20] S. Bae, Y.G. Yoo, J. Park, et al., Chem. Commun. 53 (2017) 11767–11770.
[21] D.A. Agyeman, M. Park, Y.M. Kang, J. Mater. Chem. A 5 (2017) 22234–22241.
[22] R. Liu, Y. Lei, W. Yu, et al., ACS Energy Lett. 2 (2017) 313–318.
[23] C. Zhu, Y. Wang, L. Shuai, et al., Chin. Chem. Lett. 31 (2020) 1997–2002.
[24] Z. Wang, D. Xu, J. Xu, X. Zhang, Chem. Soc. Rev. 43 (2014) 7746–7786.
[25] J. Long, Z. Hou, C. Shu, et al., ACS Appl. Mater. Interfaces 11 (2019) 3834–3842.
[26] R. Bi, G. Liu, C. Zeng, et al., Small 15 (2019)1804958.
[27] X. Li, C. Wen, H. Li, G. Sun, J. Energy Chem. 47 (2020) 272–280.
[28] G. Liu, L. Zhang, S. Wang, L.X. Ding, H. Wang, J. Mater, Chem. A 5 (2017) 14530–14536.
[29] H. Gong, H. Xue, T. Wang, et al., ACS Appl. Mater. Interfaces 8 (2016) 18060–18068.
[30] Y. Ren, S. Zhao, H. Li, et al., J. Energy Chem. 30 (2019) 63–70.
[31] Q. Liu, J. Xu, Z. Chang, X. Zhang, J. Mater. Chem. A 2 (2014) 6081–6085.
[32] L. Shang, H. Yu, X. Huang, et al., Adv. Mater. 28 (2016) 1668–1674.
[33] Y. Tu, H. Li, D. Deng, et al., Nano Energy 30 (2016) 877–884.
[34] Z. Sun, L. Lin, M. Yuan, et al., Electrochim. Acta 281 (2018) 420–428.
[35] J. Zhang, C. Dong, Z. Wang, et al., Electrochim. Acta 284 (2018) 495–503.
[36] B.R. Jia, M.L. Qin, S.M. Li, et al., ACS Appl. Mater. Interfaces 8 (2016) 15582–15590.
[37] M. He, P. Zhang, L. Liu, B. Liu, S. Xu, Electrochim. Acta 191 (2016) 90–97.
[38] W.B. Luo, S.L. Chou, J.Z. Wang, Y.C. Zhai, H.K. Liu, Small 11 (2015) 2817–2824.
[39] T. Zhu, X. Li, Y. Zhang, et al., J. Electroanal. Chem. 136 (2014) 16481–16484.
[40] F. Song, X. Hu, J. Am. Chem. Soc. 136 (2014) 16481–16484.
[41] L.J. Zhang, R. Zheng, S. Li, et al., ACS Appl. Mater. Interfaces 6 (2014) 13406–13412.
[42] S.U. Lee, R.V. Belosludov, H. Mizuseki, Y. Kawazoe, Small 5 (2009) 1769–1775.
[43] Q. Li, P. Xu, W. Gao, et al., Adv. Mater. 26 (2014) 1378–1386.